frontiers | Frontiers in Earth Science

TYPE Original Research
PUBLISHED 07 May 2025
DOI 10.3389/feart.2025.1594518

OPEN ACCESS

EDITED BY
Xiaojun Feng,
China University of Mining and Technology, China

REVIEWED BY
Kesong Fan,
Henan Polytechnic University, China
Qingwen Shi,
North China Institute of Science and Technology, China

*CORRESPONDENCE
Chenyang Zhang,
zcy579@126.com

†These authors share first authorship

RECEIVED 16 March 2025
ACCEPTED 10 April 2025
PUBLISHED 07 May 2025

CITATION
Gao F, Zhang C, Han L, Xia Y, Gao Q, Zhou Y and Li D (2025) Study on the evolution law of acoustic emission time series characteristics of coal-rock assemblage under true triaxial conditions.
Front. Earth Sci. 13:1594518.
doi: 10.3389/feart.2025.1594518

Study on the evolution law of acoustic emission time series characteristics of coal-rock assemblage under true triaxial conditions

Fuquan Gao[1†], Chenyang Zhang[2,3*†], Lingchen Han[1], Yongxue Xia[2,3], Quanwu Gao[1], Yiqun Zhou[2,3] and Dingyi Li[2,3]

[1]China Coal Northwest Energy and Chemical Group Co., Ltd., Ordos, China, [2]Coal Mining Branch, China Coal Research Institute, Beijing, China, [3]China Coal Technology and Engineering Group (CCTEG) Coal Mining Research Institute, Beijing, China

Introduction: This study aims to investigate the fractal characteristics of acoustic emission (AE) signals during coal-rock rupture and their predictive significance for impact dynamic hazards.

Methods: True triaxial loading/unloading tests were conducted on five coal-rock composites with varying coal-thickness ratios using the TRW-3000 system, with AE signals analyzed to correlate stress evolution and temporal-spatial fractal features.

Results: Key findings reveal that: 1) AE parameters exhibit stress-dependent behavior, growing slowly initially, stabilizing during stress-holding, and surging exponentially before peak stress, with ~90% of cumulative energy released pre-destabilization; 2) Ring counts follow an Λ-type trend against absolute energy, while coal-thickness proportion induces a mirror-image N-type pattern in AE parameters; 3) High-energy/high-ringcount AE events cluster spatiotemporally before failure, with clear time sequence precursors—short-duration ground sounds and consecutive rises in energy/frequency serve as critical early-warning indicators, whereas isolated signals lack hazard relevance.

Discussion: These fractal patterns and precursor thresholds enhance real-time monitoring and risk assessment frameworks, offering actionable strategies for mitigating coal-rock dynamic disasters in underground mining.

KEYWORDS

true triaxial test, acoustic emission, coal-rock composite, coal rock rupture, temporal characteristics, rockburst

Introduction

Impact ground pressure currently poses as a significant disaster in coal mine safety production, stemming from the unstable and abrupt release of energy during the adjustment process within the coal-rock system. This transient phenomenon is closely related to the formation and development of fissures in surrounding rock (Wang et al., 2024; Qi et al., 2019; Pan et al., 2023; Dou et al., 2022; Pan et al., 2012; Zhu et al., 2020; Zhang et al., 2020;

Si et al., 2024). Acoustic Emission (AE) technology can monitor in real time the micro-vibration information of fissure gestation, generation, process of fracture, and its progression from micro-fracture to instability damage within coal rock bodies. By analyzing acoustic emission data, one can infer the damage evolution characteristics within the coal rock body, evaluate trends in its internal energy adjustments, and predict potential ground pressure disasters. Therefore, the study of acoustic emission characteristics during the rupture process of coal rock bodies holds significant importance. It holds significance for monitoring and early warning of impact ground pressure, gradually gaining attention and becoming a research focus for numerous scholars (Tang et al., 2024; Tan et al., 2000; Cao et al., 2023; He et al., 2011; Cao et al., 2007; State Administration for Market Regulation & Standardization Administration of China, 2019).

Numerous scholars have conducted extensive research on the acoustic emission characteristics during the deformation and damage of coal rock bodies, as well as on critical precursor information indicating impending failure. Cao et al. (2007) carried out the acoustic emission test under uniaxial compression on a coal body, and proposed to use the acoustic emission event rate, ringing event ratio and cumulative AE ringing counts to characterize the acoustic emission trend during the deformation and damage process of the coal body. Liu et al. (2009) conducted acoustic emission tests on coal rock subjected to uniaxial compression, formulated a damage model based on its acoustic emission characteristics, and derived damage evolution curves and equations. Zhang (2018) carried out acoustic emission tests on raw coal and type coal under two conditions of conventional triaxial loading and axial pressure unloading, and analyzed the acoustic emission characteristics of different types of coal samples during deformation and damage and their differences, and found that the raw coal showed brittle deformation characteristics after the peak, and the peak value of acoustic emission indexes appeared before the peak stress, and the type coal showed ductile deformation of plastic flow after the peak, and the peak value of acoustic emission indexes appeared after the peak stress. Ding et al. (2019) carried out uniaxial compression acoustic emission tests on complete high-strength coal samples, medium-strength coal samples with fissures or gangue, and low-strength coal samples with fissures and weak gangue, compared and analyzed the characteristic parameter laws at the acoustic emission signal surge point and the stress peak point, and introduced wavelet analysis to obtain the acoustic emission characteristics of the time-frequency domain at the above two points. Li et al. (2004) studied the deformation and acoustic emission characteristics of uniaxially compressed rocks during the damage process, and found that the acoustic emission event rate of rocks increased with the increase of the stress level in the elastic phase, while the acoustic emission event rate of some rock samples showed a significant decrease near the peak intensity, i.e., a period of relative calmness occurred; Song et al. (2017) investigated the evolution of deformation localization during the deformation evolution of rocks under uniaxial compression, Cao et al. (2019) explored the influence of various loading rates on the mechanical behavior, acoustic emission patterns, and damage progression of rocks subjected to uniaxial compression, as supported by studies that highlight the correlation between acoustic emission parameters and the phases of rock damage evolution. Song et al. (2020) explored the acoustic emission characteristics of weakly cemented rocks with varying grain sizes during uniaxial compression, identifying damage precursor information by analyzing the peak frequency of AE signals. Yang et al. (2022) investigated the acoustic emission characteristics of weakly cemented rocks of different grain sizes in uniaxial compression and gave a method for identifying damage precursor information based on the peak frequency of AE. The acoustic emission signals of tungsten rock and sandstone under uniaxial compression were investigated by Yang et al. (2022), and the HPWVD algorithm was used to obtain the time-frequency characteristics of the acoustic emission signals before and after the critical point; Peng et al. (2023) investigated the acoustic emission characteristics of five different sizes of rock specimens under uniaxial compression, and analyzed the influence of the size effect on the characteristic parameters of the acoustic emission; Wang and Yuan (2023) conducted a study on the acoustic emission characteristics of rock under uniaxial compression, revealing that different loading rates significantly affect the acoustic emission signals, energy release, and failure modes of the rock. performed uniaxial compression acoustic emission tests on rocks subjected to varying loading rates, examining the impact of loading rate on the nucleation mechanism of rock microfracture agglomeration and the evolutionary characteristics of multiple types of fracture sources; Cao et al. (2015) explored the evolution of acoustic emission characteristic parameters in rocks subjected to uniaxial compression at varying loading rates, subsequently developing a damage evolution model grounded in AE ringing phenomena; Zuo et al. (2011) conducted a study on the acoustic emission characteristics during uniaxial compression, focusing on parameter analysis; examined the acoustic emission properties and three-dimensional spatial distribution patterns of rock specimens, coal specimens, and coal-rock assemblages at various phases. Ji and Lu (2015) carried out conventional triaxial compression acoustic emission tests on rocks with different peripheral pressures, and investigated the correspondence of the characteristic parameters of the low-frequency and high-frequency signals of the acoustic emission with the stresses and time in the whole process of rock rupture; Peng et al. (2024) investigated the influence of the inclination angle of the structural surface of coal-rock assemblage on the AE ringing counts during true triaxial loading and unloading tests.

In summary, most of the previous research objects are pure coal, pure rock or coal-rock composite cylinders, typically, uniaxial or conventional triaxial compression methods are employed, yet replicating intricate downhole stress conditions remains challenging. Hence, the author conducted a true triaxial loading and unloading acoustic emission test, focusing on coal-rock composite squares with varying coal thickness ratios as the research parameter utilizing the acoustic emission system to monitor the whole process, and analyses the information of critical damage precursors of coal-rock composite with different coal-thickness ratios, which is aimed to provide guidance for the evaluation of the impact ground pressure risk and the monitoring of the early warning.

Specimen preparation and test programme

Specimen preparation

The coal rock samples utilized for testing originated from an impact ground pressure mine situated in the Ordos Basin. Table 1 presents the fundamental physic-mechanical properties of the coal

TABLE 1 Basic physical and mechanical parameters of coal rock samples.

Categories	Blind spot/kg·m^{-3}	Uniaxial compressive strength/MPa	Modulus of elasticity/GPa	Poisson's ratio
Coal	1293.22	19.37	2.65	0.33
Rock	2435.64	28.75	8.51	0.26

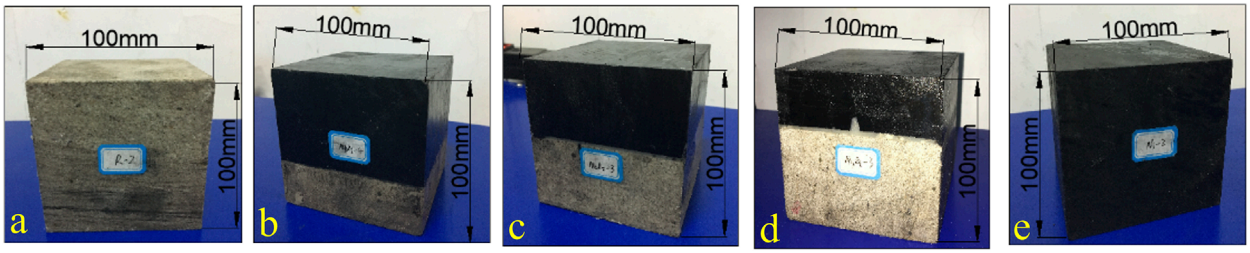

FIGURE 1
Prepared experimental samples, **(a)** The thickness of coal sample is 0%, **(b)** The thickness of coal sample is 33%, **(c)** The thickness of coal sample is 50%, **(d)** The thickness of coal sample is 67%, **(e)** The thickness of coal sample is 100%.

rock body, while the lithology of the samples is identified as medium sandstone. Each specimen measures 100 mm × 100 mm × 100 mm, with coal body thickness ratios varying at 0%, 33%, 50%, 67%, and 100%. Specimens of pure coal bodies and pure rock bodies underwent direct cutting and processing to adhere to the specified requirements; for coal-rock assemblage, mica glue is used to bond the coal body and rock body, the bonding thickness is controlled to be less than 0.5 mm, dry naturally for 24 h to complete the curing, the end face is not parallel to the degree of less than 0.01 mm, and the perpendicularity error between the end face and the axis is less than ±0.25°. The specimens, prepared in accordance with the GB/T 16773-2008 standard for coal petrographic analysis, are displayed in Figure 1.

Test equipment

The TRW-3000 rock true triaxial electro-hydraulic servo test system was utilized for the test, featuring a fully digital acoustic emission monitoring system and equipped with an automatic servo system for precise position and signal reception. This system, as detailed in the study (Du et al., 2014), is capable of assessing the strength and deformation characteristics of materials under true triaxial conditions, as demonstrated in the research conducted at the China University of Mining and Technology (Dou et al., 2022). The test system can achieve three-way six-sided independent loading and unloading, the maximum load of up to 3000 kN, the resolution of 20N, extensometer measurement range of 0–10 mm, resolution accuracy of 0.0005 mm. The acoustic emission monitoring system features six channels, with a monitoring frequency range of 20 KHz to 1200 KHz, and a specified threshold value. 40 dB. To guarantee complete contact between the specimen and the pressure plate of the loading device, a matching loading mold is utilized. A matching loading mold was fabricated in advance to match the specimen size. A space has been reserved around the mold for a steel plate to be placed in contact with the pressure block of the tester. Three extensometers are mounted on the surface of the steel plate, and six acoustic emission probes are fixed to the pressure plates in front of, behind, to the right, to the left, to the top and to the bottom of the annular pressure cylinder using petroleum jelly. The test loading mold and loading system are shown in Supplementary Figure S1.

Test programme

The test stress path is formulated according to the evolution characteristics of the stress field of the surrounding rock in the underground mining roadway. That is, before the roadway is excavated, the coal rock body is under the three-way stress state of the original rock; after the roadway is excavated, the coal rock of the bottom plate becomes a free surface, which causes the horizontal direction stress perpendicular to the airspace surface to be unloaded, and the stress field of the airspace surface is transformed from the three-way stress state to the two-way stress state; with the advancement of the mining workface, the vertical direction stress receives superimposed influence under the influence of the mining stress. Therefore, the 'horizontal unloading + vertical loading' stress path is set to simulate the on-site stress field.

To accurately investigate the mechanical properties of the coal rock mass under true triaxial stress conditions, the initial stress state was established using the measured *in-situ* stress values from the sampling mine. Specifically, the maximum horizontal principal stress, minimum horizontal principal stress, and vertical principal stress were measured as 12 MPa, 6.75 MPa, and 7.5 MPa, respectively. The true triaxial stress loading path is divided into 5 stages: stage A loading initial stress (load σ1, σ2, σ3 to 6.75Mpa at a rate of 0.1 MPa/s, keep σ3 constant, load σ1, σ2 to 7.5 MPa at a rate of 0.1 MPa/s; keep σ2, σ3 constant, load σ1 to 12 MPa at a rate of

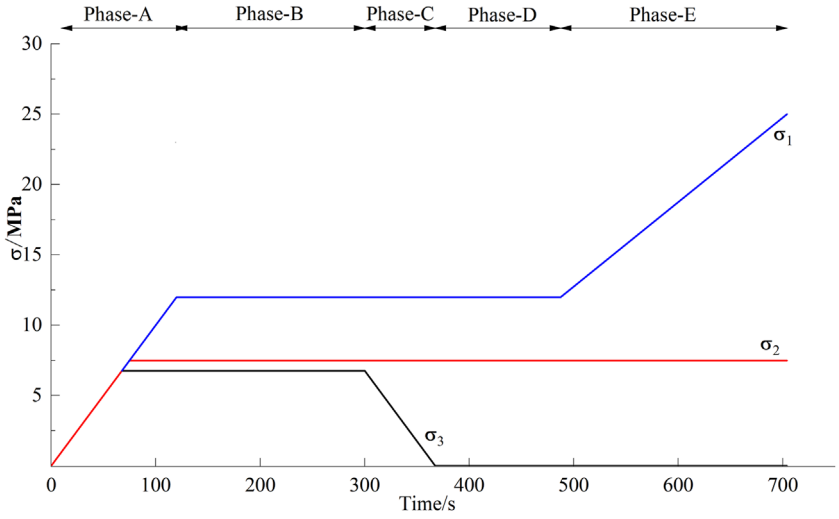

FIGURE 2
True triaxial stress loading path.

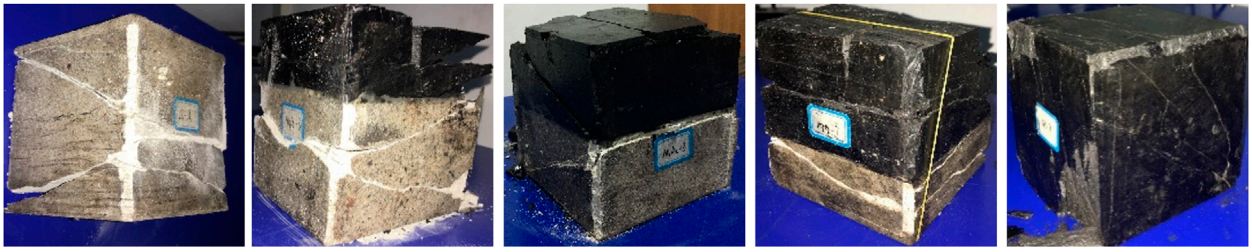

FIGURE 3
Sample after loading damage.

0.1 MPa/s), stage B Maintain the initial stress stable for a period of time (keep σ1, σ2, σ3 unchanged and maintain stability for 3 min), Stage C unload σ3 to 0 (keep σ1, σ2 unchanged and unload σ3 to 0 at a rate of 0.1 MPa/s), Stage D maintain the stress stable for a period of time (keep σ1, σ2, σ3 unchanged and maintain stability for 2 min), and Stage E load σ1 to the destruction of the specimen (load σ1 at a rate of 0.1 MPa/s rate loading σ1 to specimen destruction). As shown in Figure 2, the σ1 surface is loaded with destructive stress, the σ2 surface is loaded with minimum horizontal principal stress, and the σ3 surface is the critical surface for stress unloading.

In the test, a fixed load rate (0.1 MPa/s) was used for loading and unloading, with each type of specimen undergoing three tests. The test concluded when the specimen could no longer withstand the maximum compressive stress. Throughout the test, acoustic emission signals and force deformation data were continuously monitored, for analysis, the average of the monitoring data obtained from these three tests (with a standard deviation of less than 5%) was utilized. Figure 3 shows the damage pattern of the specimen at the end of the test.

Analysis of basic characteristic parameters of AE

AE ring count analysis

The AE ringer count represents the frequency of acoustic emission signal oscillations crossing the threshold per unit time, indicating the extent of damage cracks formed during the specimen's failure process. The higher the ringing count, the more serious the internal damage of the specimen. Figure 4 shows the variation curves of maximum principal strain (Z direction) and ringing count with loading time during true triaxial loading of specimens with different coal thickness ratios. In Figure 4, the phases A, B, C, D, and E represent the stress loading and unloading phases, respectively, and the subsequent figures follow the same convention.

Figure 5 illustrates the relationship between accumulated ring counts and specimens featuring various coal thickness ratios across different loading phases, while Figure 6 compares the maximum and cumulative ringing counts among these specimens.

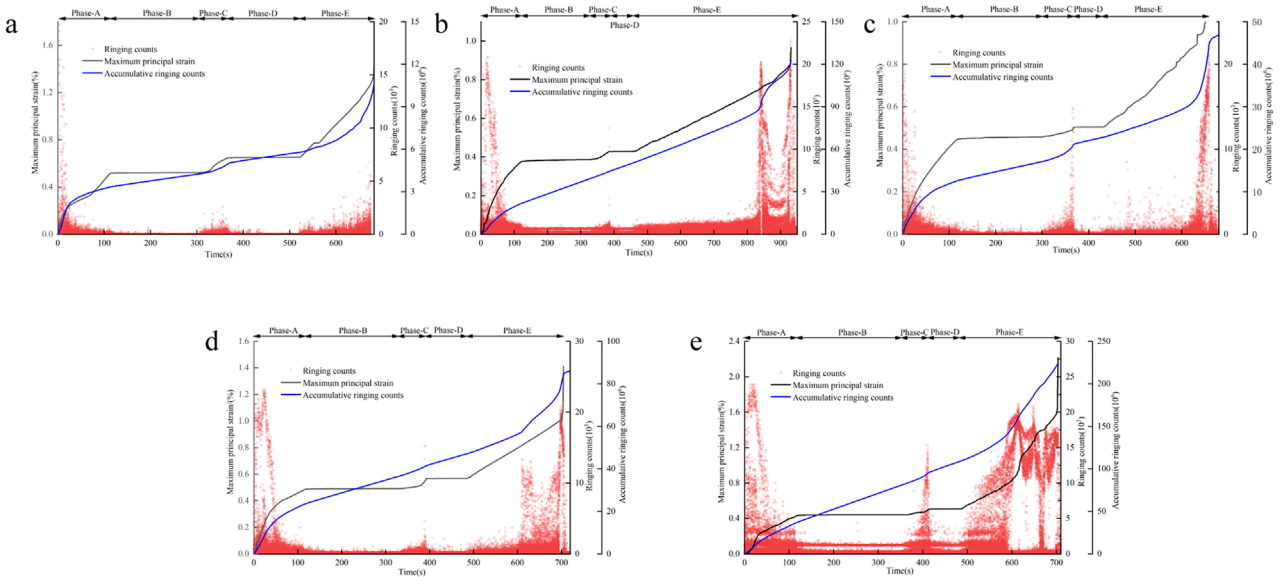

FIGURE 4
The relationship between maximum principal strain and time and ringing counts, **(a)** The thickness of coal sample is 0%, **(b)** The thickness of coal sample is 33%, **(c)** The thickness of coal sample is 50%, **(d)** The thickness of coal sample is 67%, **(e)** The thickness of coal sample is 100%.

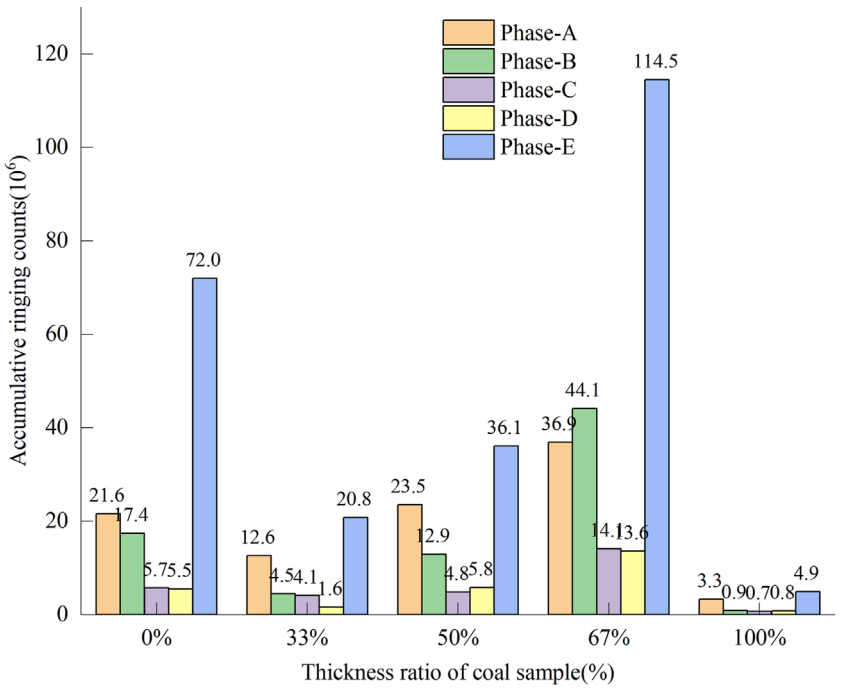

FIGURE 5
The relationship between accumulative ringing counts and thickness ratio of coal sample at different loading phase.

Comprehensive Figures 6–8 combined with comparative analysis show that:

(1) Regarding the timing characteristics of AE ringing counts, the timing characteristics of AE ringing counts of specimens with different coal thickness ratios are basically the same, which are described as follows: In phase A, the initial phase of stress loading corresponds to the compaction phase, where cracks within the specimen undergo gradual compaction and closure. This is accompanied by a rapid and stable rise in AE ringing counts and maximum principal strains. Subsequently, the loading process transitions into the elasticity phase,

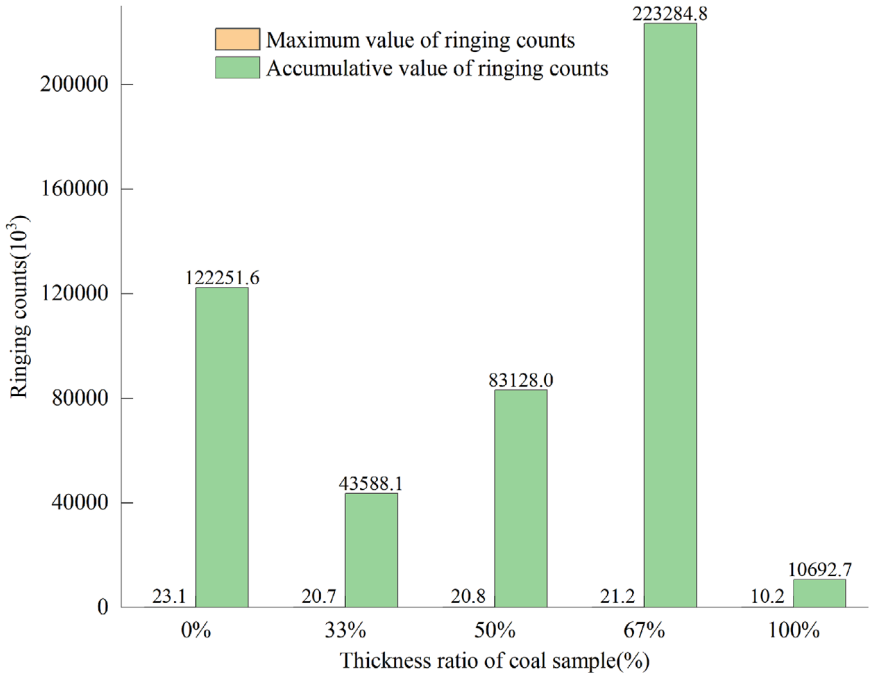

FIGURE 6
The relationship between maximum value of ringing counts and accumulative value of ringing counts and thickness ratio of coal sample.

characterized by a slower increase in AE ringing counts and maximum principal strains, with a notably reduced gradient. Then, the loading process proceeds into the elastic phase. G counts and maximum principal strain increased slowly, and the gradient of the increase decreased significantly. In phase B, the stress environment of the specimen remained stable, the AE ring counts were maintained at a low level and remained stable, and the maximum principal strain remained stable. In phase C, the X-direction stress is released, causing damage to the specimen's stress environment. Consequently, new cracks emerge within the coal rock, accompanied by a rapid surge in AE ringing counts and maximum principal strain, marked by a transient, abrupt increase. In phase D, the stress environment of the specimen remains stable, with AE ringing counts maintained at a consistently low level. Similarly, the maximum principal strain remains unchanged and stable. In phase E, stress is continuously applied until the specimen sustains damage, with the maximum principal strain gradually increasing at a stable rate until it sharply rises in a straight line just before damage occurs. For the AE ringing counts, the trend of different coal thickness proportion specimens is basically the same, and there are some differences in the detailed characteristics: for the pure rock (0% coal thickness proportion) specimen. In the early phase, AE ringing counts remain stable with negligible increase; subsequently, they surge sharply, decline, and then rise abruptly until the specimen is destroyed and destabilized. It can be seen that, after the preloading, the internal cracks of the specimen have been completely closed, the specimen has entered the phase of plastic damage, the internal micro-cracks are fully developed, expanded, and penetrated into the structural cracks, resulting in a sharp rise in the AE ringing counts, but the specimen still retains its load-bearing capacity; This was followed by a second sharp increase in AE ringing counts, signifying the renewed formation of internal micro-cracks due to accumulation, which was accompanied by structural cracks, eventually resulting in destructive instability. Regarding the assemblage sample with 33% coal thickness, AE ring counts rose slowly and steadily in the initial phase, followed by a brief, sharp increase immediately prior to the specimen's failure. For 50 per cent of the assemblage specimens, the AE ring counts increased gradually with ups and downs in the early phases, then rose sharply and remained there for a certain period of time, and then rose sharply for a short period of time at the instant before specimen destruction. For the 67% assemblage, the AE ring counts increased rapidly for a short period of time and then remained volatile until the specimen was destabilized. For the pure coal body specimen (100% coal thickness), the AE ringing counts continued to increase in small increments with sporadic large count events until the specimen was destabilized.

(2) The AE ringing counts closely correlate with the maximum principal strains, indicating crack formation and energy release within the specimen, which subsequently leads to deformation. As the maximum principal strain rises, the AE ringing counts increase in tandem, with a consistent gradient between the two. When the maximum principal strain stabilizes, the AE ringing counts remain relatively constant. Upon an abrupt increase in the maximum principal strain, the AE ringing counts increase sharply synchronously.

(3) Regarding the correspondence between the AE ringing counts and the stress environment, the AE ringing counts mainly occurred in the phase of stress environment change, i.e., phase E (σ1 surface stress loading) and phase A (initial stress loading), which accounted for 60% and 30% of the cumulative AE ringing counts of the whole phase, respectively.
(4) Regarding the relationship between the maximum value of AE ringing counts and the cumulative value, the maximum value of AE ringing counts accounted for about 0.01%~0.05% of the cumulative value of the whole phase, which is almost negligible, indicating that a single instantaneous increase in AE ringing counts is not a precursor information of destabilization and damage, and that a sustained increase in AE ringing counts over a short period of time is the precursor of destabilization and damage of the specimen.
(5) Regarding the relationship between the maximum and cumulative values of AE ringing counts and the proportion of coal thickness, the maximum values of AE ringing counts of the samples with 0%, 33%, 50%, and 67% coal thickness ratios are about 20,000, which is twice as much as the maximum value of 10,000 of AE ringing counts of the sample with a pure body of coal (with a proportion of 100% coal thickness); the cumulative value of AE ringing counts of the sample with a pure body of coal (with a proportion of 100% coal thickness) has the lowest value, and the cumulative value of AE ringing counts of the sample with a proportion of 67% coal thickness has the lowest value. The lowest cumulative value of AE ringing count of pure coal body (100% coal thickness ratio) specimen and the highest cumulative value of AE ringing count of 67% coal thickness ratio combination body specimen, the highest value is about 20 times of the lowest value; the cumulative value of AE ringing count of 33% and 50% coal thickness ratio specimen is 4, 8 times of that of the pure coal body (0% coal thickness ratio) specimen, and 0.36, 0.68 times of that of the cumulative ringing count of the pure rocky body (0% coal thickness ratio) specimen, respectively.

AE absolute energy analysis

As discussed in the references, this work involves the study of frequency band energy characteristics of AE signals from coal body rupture in gas environments, energy evolution under different gas pressures, and the application of AE signal parameters for predicting the risk of coal and gas outbursts.

AE absolute energy is the real value of the impact signal energy of the acoustic emission event per unit time, which can reflect the energy released when the damage cracks are generated in the damage process of the specimen. As demonstrated by AE studies, specimens exhibit a direct correlation between the absolute energy of AE signals and the severity of internal damage. Figure 7 shows the variation curves of the maximum principal strain (Z-direction) and absolute energy with loading time during the true triaxial loading of specimens with different coal thicknesses. In Figure 7, in order to facilitate the comparative analysis, the real-time and cumulative units of AE absolute energy are uniformly set to 10^{-10}J and 10^{-9}J, respectively, which causes the absolute energy curves of some intervals in Figs. (a)-(e) to be almost overlapped with the horizontal axis of the coordinate axes, but it doesn't affect the analysis of the key energy events in the process of specimen loading damage.

The relationship between the absolute energy of AE for different coal thickness ratio specimens in different loading phases versus the cumulative AE absolute energy is shown in Figure 8. Figure 9 shows the relationship between the maximum and cumulative AE absolute energy of specimens with different coal thickness ratios.

Combined with Figures 7–9 combined with the comparative analysis, it can be seen that (1) The time-sequence evolution of AE absolute energy in specimens with varying coal thickness ratios remains consistent, featuring a brief, intense release of energy prior to destructive destabilization. In the E-phase (Z-direction stress loading), each specimen releases approximately 90% of its total absolute energy, exhibiting typical mainshock characteristics (Zhu and Cheng, 2000); and the second is that the absolute energy value is stably maintained at a small level in phases B and D (stress stabilization), with no obvious increase or decrease. (2) The maximum value of AE absolute energy for specimens with varying coal thickness ratios constitutes approximately 2%–6% of the cumulative value, rendering it virtually insignificant. It is evident that a single instantaneous large energy event does not precede instability damage, whereas a short-term continuous occurrence of large energy events does precede such damage. (3) The AE absolute energy time series characteristics of specimens with different coal thickness ratios exhibit distinct differences in local detailed characteristics, primarily evident during the phase of stress environment transition. The pure rock body (0% coal thickness ratio) releases energy smoothly during the whole interval from the beginning of loading to destabilization, and the cumulative absolute energy increases slowly and steadily until a short time of exponential increase before the destruction of the specimen. This suggests that pure rock mass accumulates energy steadily until it is abruptly released upon destabilization. Assemblages with coal thickness ratios of 33%, 50%, and 67% exhibited continuous energy release, with minor fluctuations during initial loading and before significant energy release preceding destabilization. The pure coal body (100% of coal thickness) releases energy smoothly during the whole interval from the beginning of loading to destabilization, and the subsequent continuous large energy release. The results indicate that, under the same stress environment, the coal body within the coal-rock assemblage is more prone to producing microfractures and releasing energy compared to the rock body. However, its bearing capacity is relatively low, and the energy release level is correspondingly modest.

Correlation analysis between acoustic emission signature parameters

The acoustic emission signal parameter distribution analysis method is to analyze the acoustic emission signal characteristic parameter values by statistical distribution. The author statistically analyzes the degree of correlation between different interval distributions of AE absolute energy, AE ringing counts, amplitude, and duration of four parameters of assemblage specimens with different coal thickness ratios, in order to analyze the correlation between acoustic emission characteristic parameters.

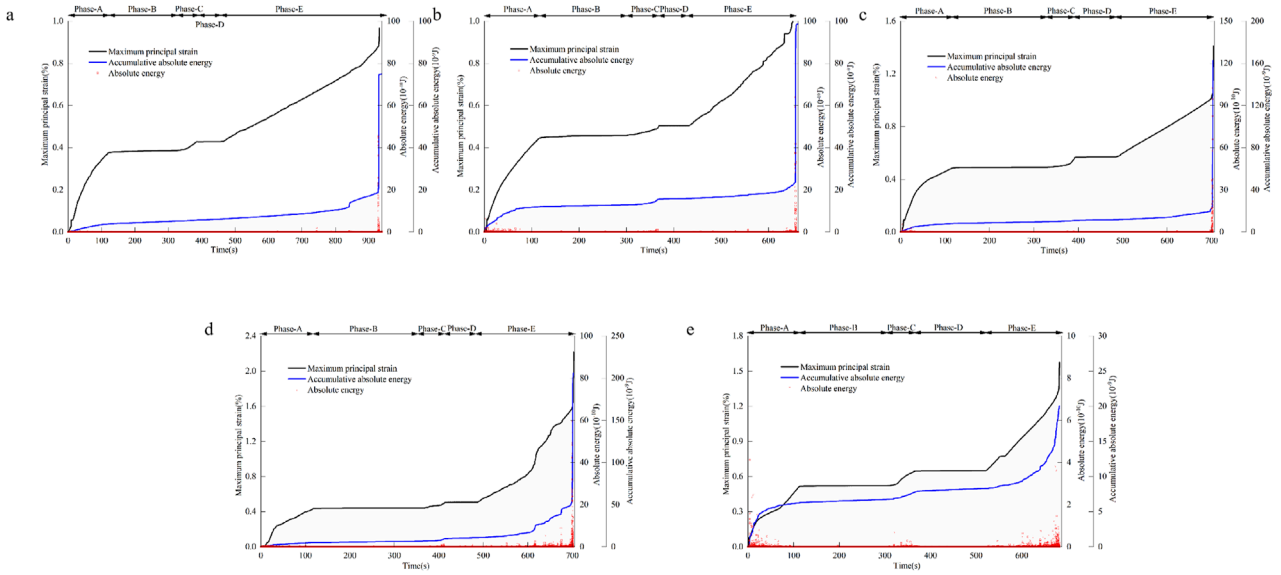

FIGURE 7
The relationship between maximum principal strain and time and absolute energy, **(a)** The thickness of coal sample is 0%,**(b)** The thickness of coal sample is 33%, **(c)** The thickness of coal sample is 50%, **(d)** The thickness of coal sample is 67%, **(e)** The thickness of coal sample is 100%.

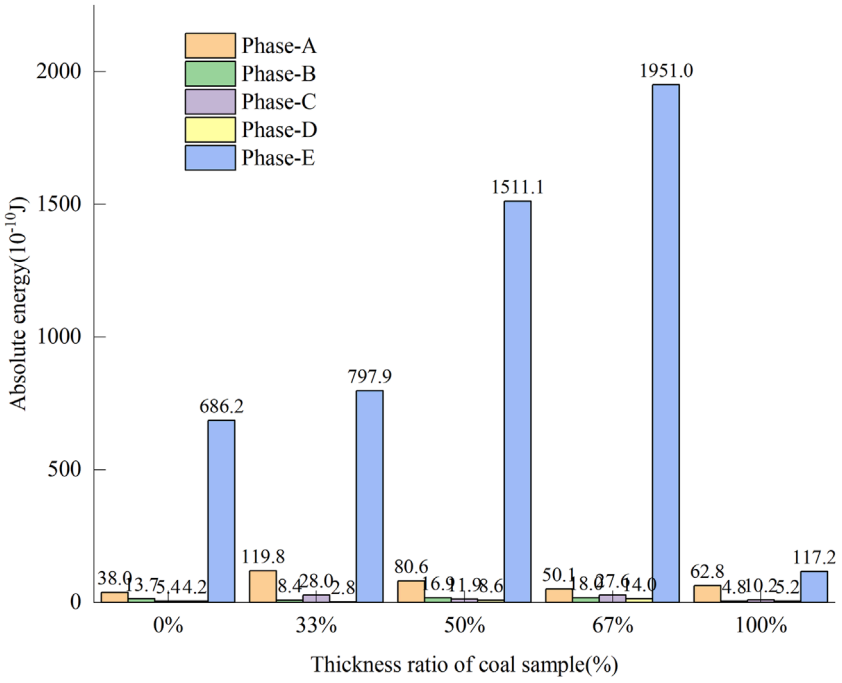

FIGURE 8
The relationship between accumulative absolute energy and thickness ratio of coal sample at different loading phase.

Correlation between absolute energy and ringing counts

Figure 10 show the comparative relationship between AE ringing counts and absolute energy distribution for different absolute energy intervals, respectively. Among them, acoustic emission events within the absolute energy interval of 0~1000aJ (1J equals 10^18aJ) are negligible due to their minute size. Hence, that portion of the data is excluded from the figure representation.

From the analysis of Figure 10a, we can see that (1) with the increase of the value of energy interval, the AE ringing counts of the samples with different coal thickness ratios show the

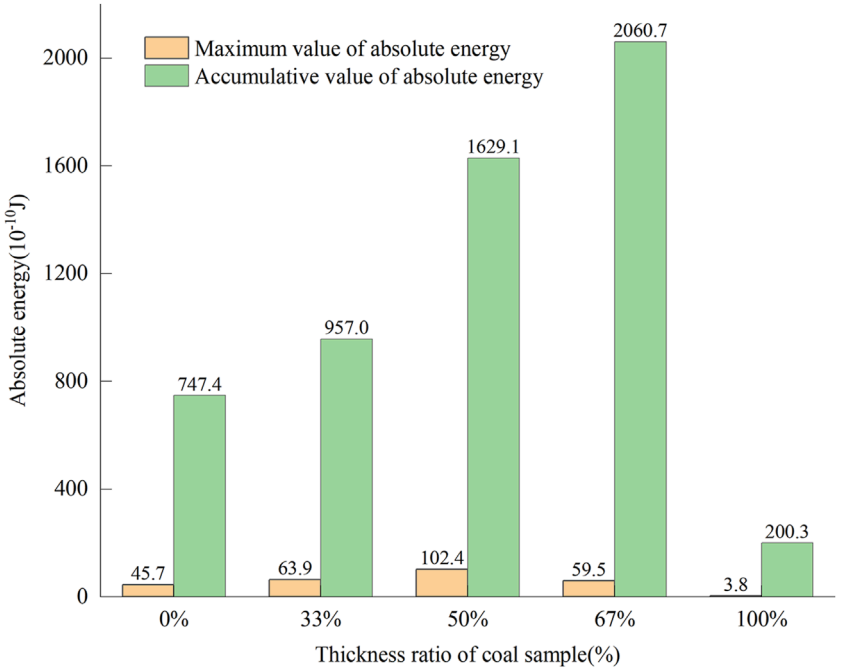

FIGURE 9
The relationship between maximum value of absolute energy and accumulative value of absolute energy and thickness ratio of coal sample.

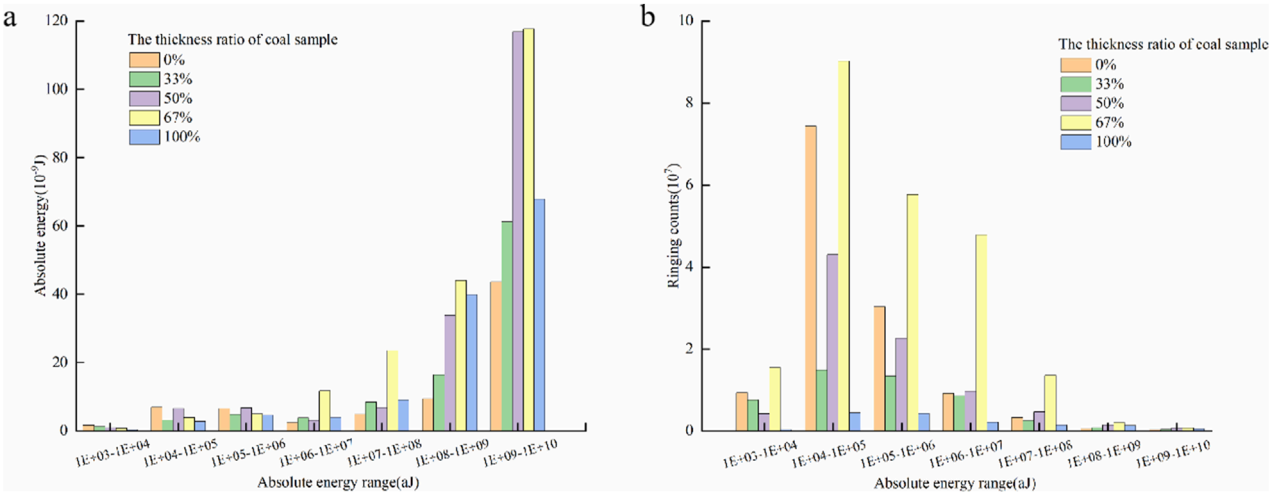

FIGURE 10
Correlation between absolute energy and ringing counts, **(a)** The distribution of ringing counts in different absolute energy range, **(b)** The distribution of absolute energy in different absolute energy range.

characteristics of increasing and then decreasing, and the whole shows the Λ-type distribution law. The study on the acoustic emission characteristics of sandy mudstone under uniaxial loading and unloading conditions reveals that AE ringing counts are predominantly distributed within the absolute energy range of 1E+04 to 1E+06aJ, with a peak in the range of 1E+04 to 1E+05aJ.(2) In the 1E+04-1E+06aJ absolute energy interval, as the proportion of coal thickness increases, the ringing counts show the characteristics of decreasing, then increasing and then decreasing, and the whole shows the characteristics of mirror N-type distribution, and reaches the maximum value when the proportion of coal thickness is 67%.

From the analysis of Figure 10b, we can see that (1) with the increase of the value of the energy interval, the absolute energy of AE of the specimens of combinations with different coal thickness proportions firstly increased steadily, and then increased sharply,

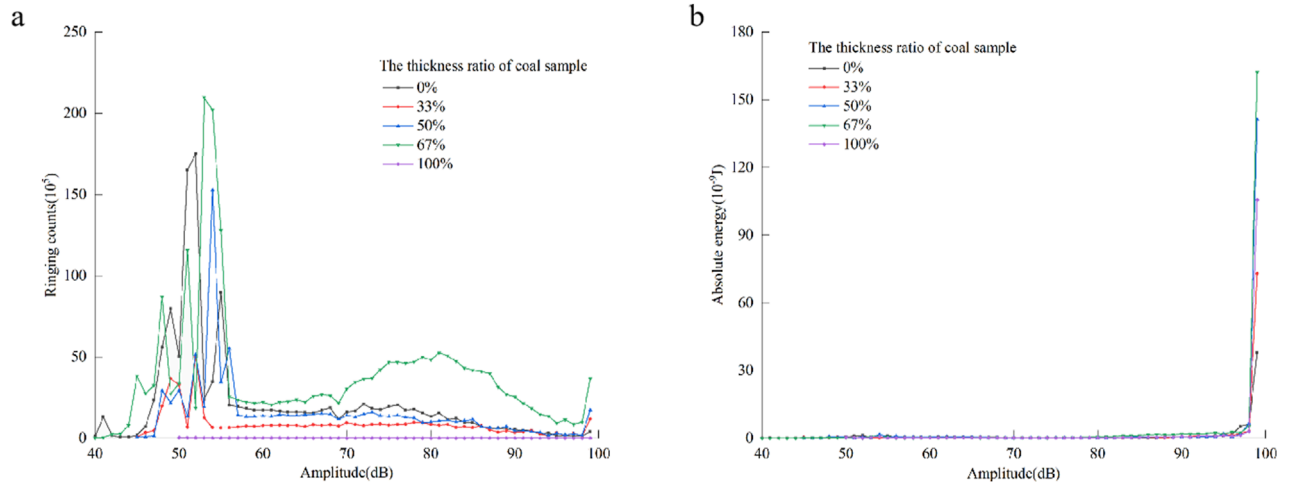

FIGURE 11
Correlation between absolute energy and ringer counts and amplitude, **(a)** The relationship between amplitude and ringing counts, **(b)** The relationship between amplitude and absolute energy.

and the whole showed an exponential distribution characteristic, and the overwhelming majority of energy was concentrated within the absolute energy range of 1E+08 to 1E+10aJ, peaking in this interval. (2) In the absolute energy interval of 1E+08~1E+10aJ, the absolute energy increases and then decreases with the increase of the proportion of coal thickness, and the whole shows a Λ-type distribution law, and reaches the maximum value when the proportion of coal thickness is 67%.

Correlation between absolute energy and ringer counts and amplitude

Acoustic emission amplitude is the maximum amplitude value of the signal waveform, which is not affected by the threshold and can be used to reflect the intensity of acoustic emission events. Figure 11 show the distribution of AE amplitude and ringer counts, and the distribution of AE amplitude and absolute energy for specimens with different coal thickness ratios, respectively.

Through a comprehensive analysis of Figure 11, we can observe that (1) For combined samples with varying coal thickness proportions, the corresponding characteristics of AE ringing counts, in terms of amplitude distribution, remain consistent, primarily concentrating within the 50–55 dB range. Furthermore, the 67% coal thickness sample exhibits a significant number of AE ringing counts within the 70–90 dB range. Notably, at an amplitude of 100 dB, the AE ringing counts of the specimens undergo a sharp increase. (2) The corresponding characteristics of AE absolute energy distribution with amplitude are the same for assemblies with different coal thickness ratios, in the amplitude range of 40–95 dB, the AE absolute energy is close to 0 value, and increases sharply at the amplitude of 100 dB, reaching a great value, which is in line with the evolution law of AE ringing counts.

Correlation between absolute energy and ringing counts and duration

Acoustic emission duration is the time from when the acoustic emission signal crosses the threshold for the first time to when it finally falls down to the threshold, which can reflect the activity frequency of acoustic emission events. The longer the duration, the higher the damage crack activity within the specimen. Figure 12 show the distribution of AE duration and ring counts, and the distribution of AE duration and absolute energy for specimens with different coal thickness ratios, respectively.

Comprehensive analysis of Figure 12 reveals that AE characteristics—amplitude, count, duration, and energy—are apt for assessing phased damage in concrete under uniaxial tension, as shown in systematic studies. (1) The distribution of AE ringing counts with the duration of the assemblage samples with different coal thickness proportions has the same characteristics, and they are mainly concentrated in the 1E+03-1E+04μs duration interval. Meanwhile, the AE ringing counts of 67% of the assemblage specimens showed a dispersed and concentrated phenomenon, which was significantly higher than the other intervals in the 1E+04-2E+04 and 8E+04-∝μs duration intervals. (2) In each duration interval, the AE ringing counts decreased and then increased with the increase of coal thickness ratio. The AE ringing counts for pure coal body samples approached zero when compared to other assemblage samples; the AE ringing counts of the pure rock body samples were higher than those of the assemblage samples with 33% and 50% coal thickness proportions, however, they were lower than those of assemblage samples containing 67% coal thickness proportions. (3)The absolute energies of AE from assemblage specimens with varying coal thickness ratios are predominantly concentrated within the 1E+05 to ∝μs duration range, while those in other intervals constitute a negligible fraction. Within the 1E+05 to ∝μs duration interval, pure coal samples demonstrate virtually zero AE absolute energy when compared to other assemblage samples.

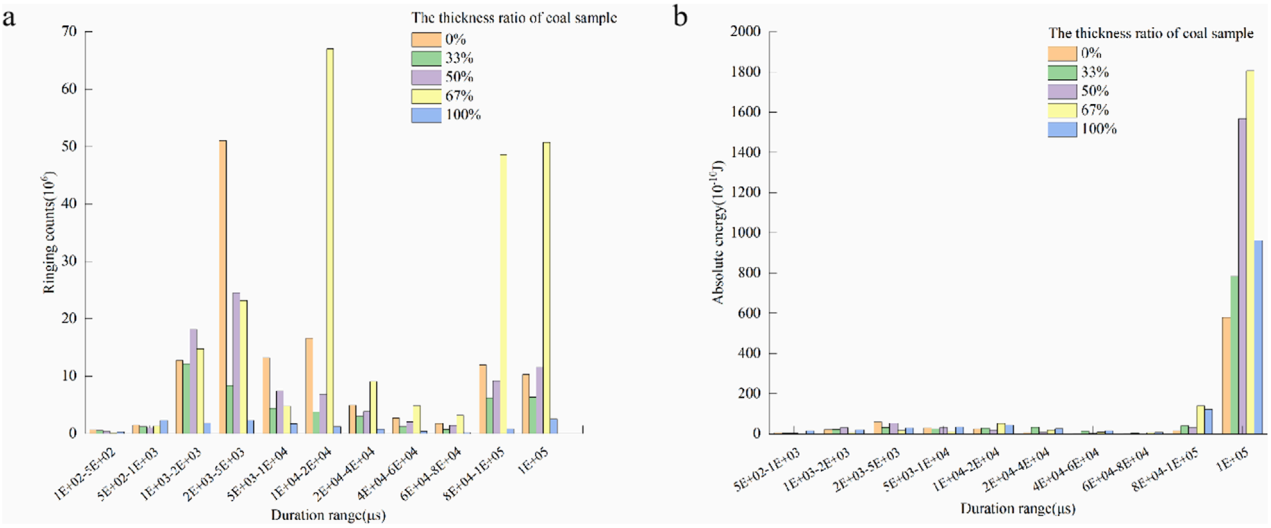

FIGURE 12
Correlation between absolute energy and ringing counts and duration, **(a)** The distribution of ringing counts in different duration range, **(b)** The distribution of absolute energy in different duration range.

As the proportion of coal thickness increases from 0% to 67%, a gradual increase in AE absolute energy is observed.

Acoustic emission characteristic parameters critical damage time sequence characteristics

Figure 13 presents the cumulative loading duration, the time point of maximum ringer count, and the time of peak absolute energy for samples with varying coal thickness ratios, Figure 14a compares the maximum absolute energy values of samples with different coal thickness ratios to the absolute energy at the time of maximum ringer count, Figure 14b illustrates the comparison between the maximum ringer count and its corresponding peak absolute energy, versus the overall absolute energy samples with different coal thickness ratio. Figure 14b shows the comparison between the maximum value of ringing counts and the absolute energy at the time of maximum ringing counts for different coal thickness ratio samples.

Comparative analyses of Figures 13, 14 show that (1) acoustic emission events with high energy and high ringer counts occur instantly before the destabilization of the specimens, and the two do not coincide. Samples with 0% and 33% coal thickness firstly experience high ringing counts and then high absolute energy acoustic emission events. Specimens with 50%, 67%, and 100% coal thickness first experienced acoustic emission events with high absolute energy, followed by acoustic emission events with high ringing counts. (2) Compared with the AE absolute energy maximum, the absolute energy at the ringing count maximum is very small and almost negligible. (3) Compared to the AE ringing count maximum, the ringing count at the absolute energy maximum is about 80%, which is very high.

Discussion

Summarizing the test results, coal body thickness is a key factor influencing the mechanical properties and failure patterns of coal-rock assemblages. Pure rock specimens are hard and dense, exhibiting high bearing capacity. During loading, micro-cracks develop and interconnect, eventually leading to structural damage and specimen instability. Pure coal body specimens are typically discontinuous, characterized by inherent damage cracks and a multitude of internal micro-voids, fractures, particle cementation surface, etc., with a weak bearing capacity, and the generation and expansion of internal micro-fractures eventually lead to macroscopic material damage of the specimen. For coal-rock composite (including pure coal body), with the decrease of coal thickness ratio, the AE ringing count shows the characteristic of increasing first and then decreasing. This results from the significant disparity in bearing capacity between the coal body and rock body, accompanied by a deformation coordination process when loading coal-rock composite, particularly as the coal thickness decreases from 100% to 67% the high proportion of the coal body can provide a spatial basis for the deformation development of the specimen under the loading, and the low proportion of the rock body can provide a dielectric basis for the adjustment of the specimen's internal stresses, therefore, the specimen with the combined proportions achieves maximum deformation development, accompanied by AE ring counts reaching their peak level of deformation. Furthermore, the AE ringing count reaches a notable level of significance; Similarly, as the coal thickness ratio decreases step-by-step from 67% to 50%, and subsequently to 33%, the deformation coordination between the coal body and rock body decreases gradually, demonstrating increasingly brittle failure characteristics in the specimen, becoming more evident, thus leading to a gradual decrease in the AE ringing count.

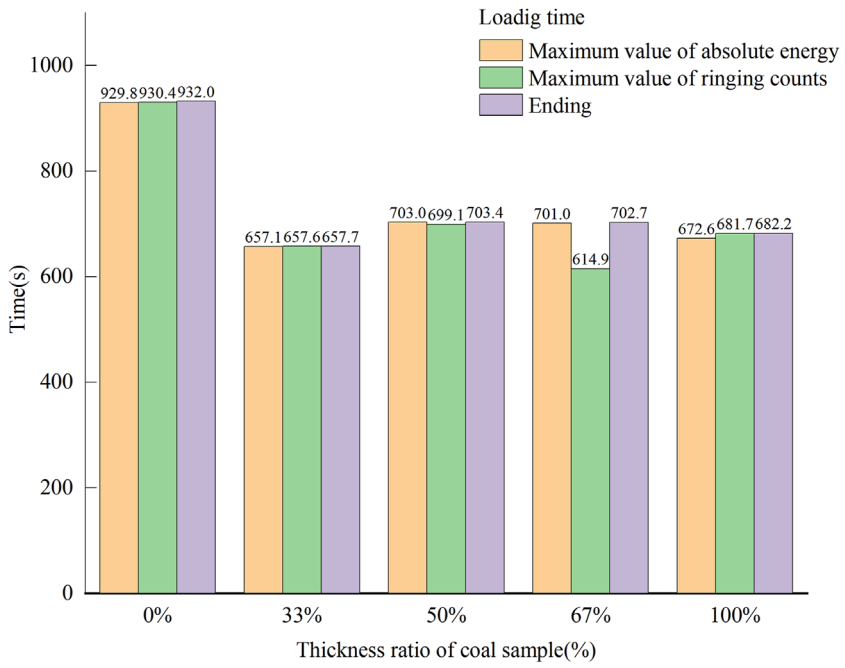

FIGURE 13
The relationship between loading time of maximum value of absolute energy and loading time of maximum value of ringing counts and ending time of loading and thickness of coal sample.

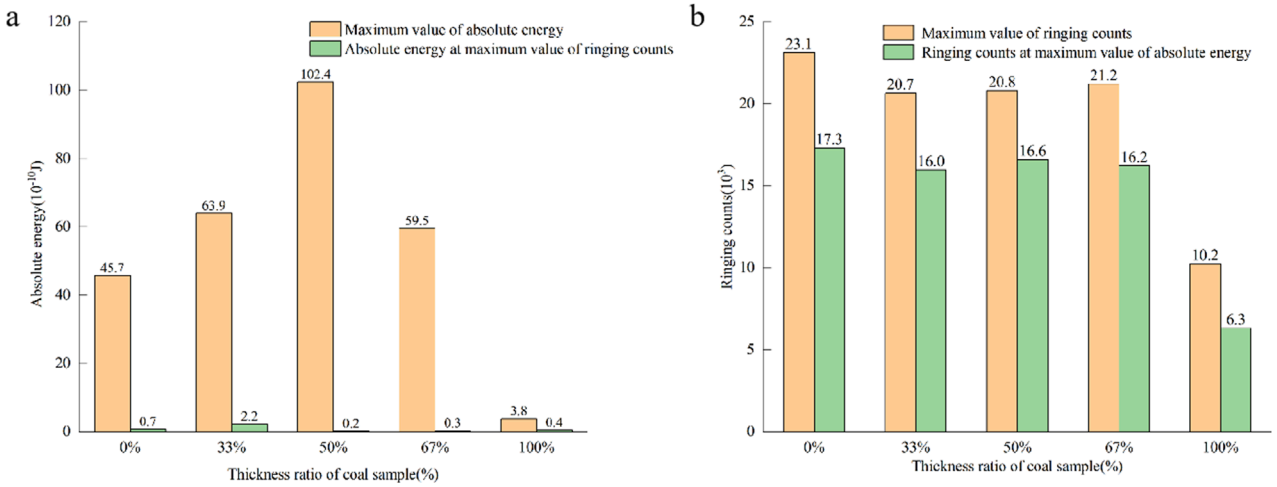

FIGURE 14
Timing of maximum value of absolute energy and maximum value of ringing counts, **(a)** The relationship between maximum value of absolute energy and absolute energy at maximum value of ringing counts and thickness of coal sample, **(b)** The relationship between maximum value of ringing counts and ringing counts at maximum value of absolute energy and thickness of coal sample.

The test results for ground sound monitoring and early warning of impact ground pressure offer certain insights, Firstly, isolated single ground sound events cannot indicate the danger of impact ground pressure, while short-duration continuous ground sound events serve as precursors to coal and rock dynamic damage. Secondly, the maximum value of ground sound energy and the peak frequency of occurrence are key indicators, highlighting the proximity of the highest values to critical thresholds. The time of the frequency of the occurrence of the ground sound energy and the frequency of the successive surge at the same time can be used as one of the precursor pieces of information for the emergence of the impact ground pressure.

Conclusion

(1) In the true triaxial loading and unloading test, the AE parameters of the samples with different coal thickness ratios have a high positive correlation with the stress environment, which increases slowly at the beginning of the loading period, does

not increase or decreases during the stress stabilization period, and then increases exponentially for a short period of time in the pre-stabilization period, and then reaches the peak value rapidly.

(2) Among the five coal-rock assemblages, the AE ringing counts, and absolute energy maxima constitute insignificant proportions compared to the cumulative values throughout the entire phase; Meanwhile, the energy released consecutively over a brief period preceding destabilization comprises approximately 90% of the total cumulative absolute energy released, exhibiting typical mainshock-like characteristics.

(3) With the increase of AE absolute energy, the ringing counts show the characteristics of increasing and then decreasing, and the overall Λ-type distribution law, which is mainly concentrated in the 1E+04-1E+06aJ absolute energy interval; with the increase of the proportion of coal thickness in the assemblage, the AE ringing counts, amplitudes and durations show the characteristics of decreasing and then increasing and then decreasing, and the overall distribution of the mirrored N-type distribution, and the maximum value is reached when 67% of the coal thickness proportion reaches the maximum value. The maximum value is reached when the proportion of coal thickness is 67%.

(4) The acoustic emission events with high energy and high ringing counts occurred at the moment before the destabilization of the specimens, which were very close to each other but did not coincide, and the absolute energy of the maximum AE ringing counts accounted for a very small proportion compared with that of the absolute energy maxima, while the ringing counts of the maximum absolute energy of the AE ringing counts accounted for 80% compared with that of the ringing counts.

(5) The temporal sequence of acoustic emission before damage of coal rock body specimens is obvious, which can provide guidance for on-site impact ground pressure monitoring. Firstly, an isolated single ground sound event cannot be used as an indicator to reflect the danger of impact ground pressure, and the short duration ground sound event is one of the precursor information of coal rock dynamic damage; secondly, the maximum value of the ground sound energy and the highest value of the frequency are highly close to each other but do not coincide with each other, and the same phase of the successive surge of the ground sound energy and the frequency can be used as one of the precursor information of the impact ground pressure manifestation.

Data availability statement

The original contributions presented in the study are included in the article/Supplementary Material, further inquiries can be directed to the corresponding author.

Author contributions

FG: Writing – original draft. CZ: Project administration, Writing – original draft, Formal Analysis, Methodology, Data curation, Visualization, Software, Supervision, Resources, Investigation, Validation, Conceptualization, Writing – review and editing, Funding acquisition. LH: Resources, Investigation, Writing – original draft. YX: Validation, Formal Analysis, Data curation, Writing – original draft. QG: Writing – original draft, Investigation, Resources. YZ: Project administration, Methodology, Writing – original draft. DL: Methodology, Project administration, Writing – original draft.

Funding

The author(s) declare that financial support was received for the research and/or publication of this article. Science Technology Innovation Foundation of CCTEG Coal Mining Research Institute in China (KCYJY-2023-QN-06); Young Elite Scientists Sponsorship Program by CAST (2023QNRC001); China Coal Group Major Science and Technology Special Project (20211BY001); National Natural Science Foundation of China (52174118); National Key Research and Development Program of China (2022YFC3004604); Science and Technology Innovation and Entrepreneurship Fund of Tiandi Science and Technology Co., Ltd. in China (2023-2-TD-ZD003).

Conflict of interest

Authors FG, LH, and QG were employed by China Coal Northwest Energy and Chemical Group Co., Ltd. Authors CZ, YX, YZ, and DL were employed by China Coal Technology and Engineering Group (CCTEG) Coal Mining Research Institute.

The authors declare that this study received funding from CCTEG. The funder had the following involvement in the study: study design, data collection, and analysis.

Generative AI statement

The author(s) declare that no Generative AI was used in the creation of this manuscript.

Publisher's note

Supplementary material

The Supplementary Material for this article can be found online at: https://www.frontiersin.org/articles/10.3389/feart.2025.1594518/full#supplementary-material

SUPPLEMENTARY FIGURE S1
True triaxial testing system, **(a)** Test loading mold, **(b)** Test loading system.

References

Cao, A. Y., Jing, G. C., Ding, Y. L., and Liu, S. (2019). Mining-induced static and dynamic loading rate effect on rock damage and acoustic emission characteristic under uniaxial compression. *Saf. Sci.* 116, 86–96. doi:10.1016/j.ssci.2019.03.003

Cao, A. Y., Jing, G. C., and Dou, L. M. (2015). Damage evolution law based on acoustic emission of sandy mudstone under different uniaxial loading rate. *J. Min. Saf. Eng.* 32 (6), 923–928.

Cao, A. Y., Liu, Y. Q., and Yang, X. (2023). Physical index and data fusion-driven method for coal burst prediction in time sequence. *J. China Coal Soc.* 48 (10), 3659–3673.

Cao, S. G., Liu, Y. B., and Zhang, L. Q. (2007). Study on characteristics of acoustic emission in outburst coal. *Chin. J. Rock Mech. Eng.* 26 (S1), 2794–2799.

Ding, X., Xiao, X. C., and Lv, X. F. (2019). Characteristics and evolution mechanism of acoustic emission time-frequency signal during coal failure process. *J. China Coal Soc.* 44 (10), 2999–3011.

Dou, L. M., Tian, X. Y., and Cao, A. Y. (2022). Present situation and problems of coal mine rockburst prevention and control in China. *J. China Coal Soc.* 47 (1), 152–171.

Du, K., Li, X. B., and Ma, C. D. (2014). Development of rock true triaxial dynamic disturbance test system and its application. *Exp. Technol. Manag.* 31 (12), 35–40.

He, H., Dou, L. M., and Gong, S. Y. (2011). Study of acoustic emission monitoring technology of rockburst. *Rock Soil Mech.* 32 (4), 1262–1268.

Ji, H. G., and Lu, X. (2015). Characteristic of acoustic emission and rock fracture precursors of granite under conventional triaxial compression. *Chin. J. Rock Mech. Eng.* 34 (4), 694–702.

Li, S. L., Yin, X. G., and Wang, Y. J. (2004). Studies on acoustic emission characteristics of uniaxial compressive rock failure. *Chin. J. Rock Mech. Eng.* 23 (15), 2499–2503.

Liu, B. X., Huang, J. L., and Wang, Z. Y. (2009). Study on damage evolution and acoustic emission character of coal-rock under uniaxial compression. *Chin. J. Rock Mech. Eng.* 28 (S1), 3234–3238.

Pan, J. F., Ning, Y., and Mao, D. B. (2012). Theory of rockburst start-up during coal mining. *Chin. J. Rock Mech. Eng.* 31 (3), 586–596.

Pan, Y. S., Song, Y. M., and Liu, J. (2023). Pattern, change and new situation of coal mine rockburst prevention and control in China. *Chin. J. Rock Mech. Eng.* 42 (9), 2081–2095.

Peng, X. Y., Gao, F. Q., and Yuan, G. Y. (2023). Experimental study on the size effect of acoustic emission characteristics of coal strain bursts. *J. Min. Strata Control Eng.* 5 (3), 033031.

Peng, Y. Y., Li, Y. F., and Yu, H. (2024). Research on mechanical properties of coal and rock with different dip angles based on true triaxial unloading test. *J. Min. Strata Control Eng.* 6 (2), 023037.

Qi, Q. X., Li, Y. Z., and Zhao, S. K. (2019). Seventy years development of coal mine rockburst in China: establishment and consideration of theory and technology system. *Coal Sci. Technol.* 47 (9), 1–40.

Si, X. F., Luo, Y., and Luo, S. (2024). Influence of lithology and bedding orientation on failure behavior of "D" shaped tunnel. *Theor. Appl. Fract. Mech.* 129, 104219. doi:10.1016/j.tafmec.2023.104219

Song, Y. M., Xing, T. Z., and Zhao, T. B. (2017). Acoustic emission characteristics of deformation field development of rock under uniaxial loading. *Chin. J. Rock Mech. Eng.* 36 (3), 534–542.

Song, Z. Y., Ji, H. G., and Zhang, Y. Z. (2020). Acoustic emission signal sources and critical failure precursors of weakly consolidated sandstone with different grain sizes. *J. China Coal Soc.* 45 (12), 4028–4036.

State Administration for Market Regulation and Standardization Administration of China (2019). *Methods for rockburst determination, monitoring and prevention—Part 5: ground sound monitoring method*. Beijing: China Standards Press.

Tan, Y. L., Li, F. C., and Zhou, H. (2000). Analysis on acoustic emission pattern for rock burst. *Chin. J. Rock Mech. Eng.* 19 (4), 425–428.

Tang, T. T., Zhao, B., and Liu, X. D. (2024). Research progress and prospects of acoustic emission detection technology in material fracture damage. *China Spec. Equip. Saf.* 40 (2), 1–7.

Wang, G. F., Pan, Y. S., and Zhao, S. K. (2024). How to realize safe-efficient-intelligent mining of rock burst coal seam. *Coal Sci. Technol.* 52 (1), 1–14.

Wang, J., and Yuan, G. T. (2023). Acoustic emission and fracture characteristics of deep sandstone under different loading rates. *J. Min. Strata Control Eng.* 5 (4), 043024.

Yang, L. R., Li, J. J., and Jiang, C., (2022). Analysis of acoustic emission parameters and time-frequency characteristics in the process of rock sample fracture. *J. Min. Strata Control Eng.* 5 (1), 013015.

Zhang, C. Y., Pan, J. F., Xia, Y. X., et al. (2020). Research on impact failure characteristics of coal-rock composite bodies under true triaxial loading and unloading conditions. *Chin. J. Rock Mech. Eng.* 39 (8), 1522–1533.

Zhang, L. (2018). Comprehensive analysis of acoustic emission evolution characteristics during deformation and failure process of outburst coal. *J. China Coal Soc.* 43 (S1), 130–139.

Zhu, S. T., Jiang, F. X., and Liu, J. H., (2020). Mechanism and monitoring and early warning technology of rock burst in the heading face of compound thick coal seam. *J. China Coal Soc.* 45 (5), 1659–1670.

Zhu, W. S., and Cheng, F. (2000). Constitutive model of energy dissipation and its application to stability analysis of ship-lock slope in Three Gorges Project. *Chin. J. Rock Mech. Eng.* 19 (3), 261–264.

Zuo, J. P., Pei, J. L., and Liu, J. F., (2011). Investigation on acoustic emission behavior and its time-space evolution mechanism in failure process of coal-rock combined body. *Chin. J. Rock Mech. Eng.* 30 (8), 1564–1570.